OPEN ACCESS

Application and Analysis of a Salt Bridge Reference Electrode Setup for PEM Water Electrolysis: Towards an Extended Voltage Loss Break Down

Journal of The Electrochemical Society, 2022 **169** 124513

Application and Analysis of a Salt Bridge Reference Electrode Setup for PEM Water Electrolysis: Towards an Extended Voltage Loss Break Down

Lena V. Bühre,[1] Sven Bullerdiek,[1] Patrick Trinke,[1] Boris Bensmann,[1,z] Anna-Lena E. R. Deutsch,[2,3] Peter Behrens,[2,3] and Richard Hanke-Rauschenbach[1]

[1]*Leibniz University Hannover, Institute of Electric Power Systems, Appelstraße 9a, 30167 Hannover, Germany*
[2]*Leibniz University Hannover, Institute of Inorganic Chemistry, Callinstraße 9, 30167 Hannover, Germany*
[3]*Leibniz University Hannover, Cluster of Excellence PhoenixD, Welfengarten 1A, 30167 Hannover, Germany*

Information on PEMWE performance is often obtained from full cell measurements. The level of detail of this information is, however, comparably low. This contribution analyzes kinetic parameters for anode and cathode reactions separately as a step towards an extended loss breakdown through a salt bridge reference electrode. The reference electrode setup is shown in detail, and qualitative measurements are discussed. OER and HER Tafel slopes and exchange current densities for both reactions are reported. An outlook on future use cases for the salt bridge reference electrode is given and supported by measurement data.
 [DOI: 10.1149/1945-7111/ac9ee1]

Manuscript submitted July 26, 2022; revised manuscript received October 6, 2022. Published December 19, 2022.

Supplementary material for this article is available online

It is imperative to investigate, understand and manage the loss mechanisms during proton exchange membrane water electrolysis (PEMWE) operation to establish the technology as an efficient tool for producing green hydrogen.[1,2] In this regard, the ability to subdivide loss mechanisms for their origin within the cell is particularly desirable. A detailed loss breakdown of the cell voltage can help better the understanding of reaction mechanisms, stability issues, and mass and charge transport phenomena.

So far, two different approaches have been used to characterize PEMWE cells. Either the conventional loss breakdown is applied, or a reference electrode (RE) is used to obtain more precise information from both half-cells. The first approach, consisting of full cell polarization curves and high-frequency resistance (HFR) measurements, is an established method to characterize PEMWE cells.[3] It leads to a conventional loss breakdown through the Tafel analysis into kinetic, ohmic, and mass transport losses.[4] Since the measured signal is limited to the full cell, the cathode activation overpotential is often assumed to be negligible compared to the anode activation.[5] Furthermore, the other losses, such as ohmic and mass transport losses, cannot be separated.

The second approach theoretically enables the kinetic, the mass transport, and the ohmic losses for both electrodes to be determined individually. Here, a RE is employed to subdivide specific loss contributions further. In the past, exemplary use cases have been the analysis of the contact resistance at the anode and porous transport layer (PTL) interface separately from the overall ohmic resistance[6] and a study of individual electrodes to assign degradation to the anode or the cathode.[7,8]

Several RE setups have been proposed throughout the past decade, but each has disadvantages. Some studies successfully test REs for PEMWE systems, but a specialized membrane electrode assembly (MEA) is required. These adaptations include a RE hot pressed between two half cells,[6] a specific geometry for the catalyst layer (CL),[9] and laser ablation of a part of the CL.[10] In other studies, the measurements have a level of uncertainty because of inhomogeneous potential distribution due to misalignment.[11] Another setup, free of the previous drawbacks, was first presented by Hinds and Brightman for fuel cells[12] and later for water electrolysis (WE).[7] Their setup consists of a salt bridge reference electrode (SBRE). The SBRE was used for cathode potential measurement during stress test (shut down) and later for current collector potential measurement in an adjusted setup.[13]

The SBRE is further elaborated in the present paper to get closer to a full loss breakdown of both electrodes separately. As a first step, kinetic losses are analyzed separately for both electrodes. For this purpose, the SBRE is successively employed on both sides (cathode and anode) and validated via measurements. A particular focus is set on the PTL preparation for SBRE application at the anode side. Finally, half-cell measurements from SBRE are used for kinetic analysis (Tafel slope and exchange current density).

The paper is structured as follows. First, the reference electrode setup is shown, and a detailed explanation of the electric and protonic potential distributions is given. This background is crucial to subsequently be able to comprehend which loss components are included in the RE measurement. Afterward, the results of the preliminary investigations are discussed. Thereafter, measurements with the RE on both sides of the cell are shown and explained with a particular focus on kinetic analysis.

Reference Electrode: Materials and Methods/Experimental

Set up and working principle.—Instead of a two-electrode measurement, the three-electrode measurement is enabled through a salt bridge located at the PTL. The PTL is impregnated with an electrolyte (Nafion™) to bridge the potential from the CL to the salt bridge. The salt bridge transmits the ionic potential outside of the cell, where it can be accessed with an external RE in an H_2SO_4 solution. Details of the setup will be provided in this section. This work acknowledges the glossary from the EU technical report on low-temperature water electrolyzers.[14]

The starting point for the setup is a PEMWE research cell manufactured by Fraunhofer ISE. The cell has an active area of 4 cm^2. Titanium current collectors and end plates equipped with flow fields are used. Details can be found in Refs.15,16. The salt bridge is integrated through one of the end plates. A hole tapped 13 mm deep with an ANSI 1⁄4–28 UNF thread is placed in the end plate. Between the thread base and the contact surface of the PTL, a hole is provided with a diameter of 1.65 mm for the hose (outer diameter 1/16 inch = 1.5875 mm). To ensure a complete screw-in, a countersink with a diameter of 10 mm and a depth of 1 mm is added to the modification. The salt bridge is integrated with the flangeless PFA hose fitting from Darwin Microfluidics in a set with the ETFE Ferrule 1⁄4 00–28

[z]E-mail: boris.bensmann@ifes.uni-hannover.de

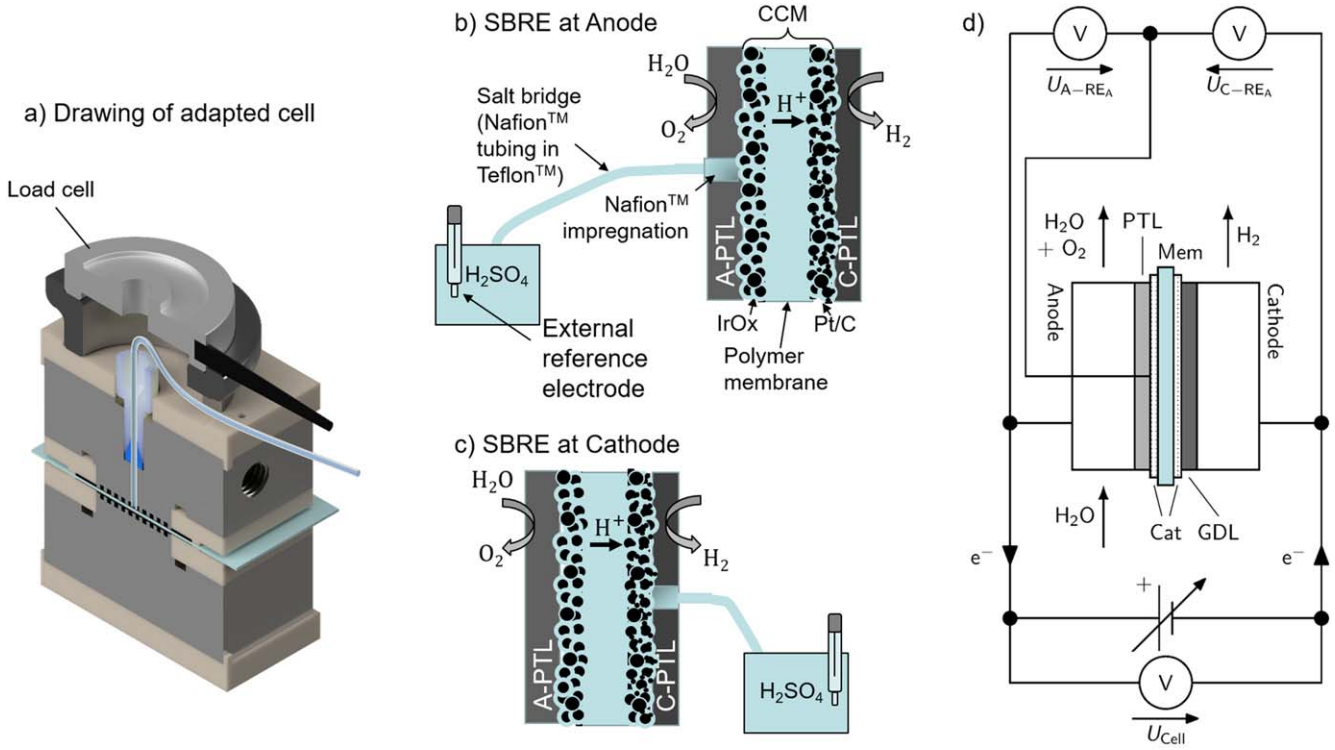

Figure 1. Setup of salt bridge reference electrode, (a) technical drawing of the modified electrolysis cell with salt bridge at flowfield and sketches of the experimental setup with RE at (b) anode and (c) cathode side of a typical 5-layer PEM water electrolysis cell. (d) Measurement specifications in RE-setup at anode from (b) with a typical 5-layer PEM water electrolysis cell.

to 1⁄16 00 OD (SKU: CIL-XP-245X). The salt bridge consists of an outer hose made of PTFE (Darwin Microfluidics (SKU: BL-PTFE-1610–20). The outer diameter is 1⁄16 inch, and the inner diameter is 1 mm. It is designed to be gas-tight to the flow field by the hose fitting. Inside is a Nafion™ hose, with an outer diameter of the Nafion™ tubing reported to be 0.762 mm to 0.914 mm depending on humidity. The inner diameter is 0.584 mm to 0.711 mm, from Gasmet. A microscope image of the salt bridge can be found in the supplementary material (SI). The system is applicable on either anode or cathode side. Figure 1a shows the technical drawing of a modified cell with the salt bridge being located in the end plate and leaving the cell from underneath the cylinder of the load cell. The load cell is a sensor for the force on the active area of the PEMWE cell and the gasket.

For a better understanding of the ionic bridge, Fig. 1b shows a typical 5-layer PEM cell with the ionic path highlighted in blue color. In the center of the cell is the PEM. It separates the cell into the anode and cathode and is conductive for protons. The cell is designed symmetrically, with the CLs on both sides next to the membrane, followed by the PTLs. PTLs used in the measurements are sintered titanium fibers on the anode (0.2 mm, 2GDL40–1.00, Bekaert), and carbon with hydrophobic treatment on the cathode (E20H (former H23i2), Freudenberg SE). While the CLs are conductive for protons, the PTL is usually not. In this setup, the anode PTL is impregnated with Nafion™ to make it conductive in the area where the salt bridge is located. The salt bridge is immersed in an H_2SO_4 filled beaker together with an external RE. The solution is a diluted sulfuric acid with a concentration of 0.5 M. The external RE is an Ag/AgCl RE from BASi with 3 mol l^{-1} NaCl solution, and the potential vs SHE is 196 mV at 25 °C. The potential of the Ag/AgCl RE depends on the temperature of the solution, increasing about 0.5–1 mV per °C.[17] In this work, a value of 1 mV $°C^{-1}$ is used for temperature correction. Data will be presented against SHE potential. Figure 1c shows the setup for a RE measurement at the cathode.

The potentiostat connections are shown in Fig. 1d. In addition to the positive and the negative connectors at the anode and cathode respectively, a reference connection is located on one of the CLs. In this study, an SP150 with 20 A Booster by BioLogic is used as the potentiostat.

The CCM and MEA materials used throughout the study are listed in Table I and will be referred to by the respective number.

Nafion™ impregnation.—Subsequently, the procedure of impregnation is outlined in detail. First, the titanium PTLs are washed in DI water in an ultrasonic bath for 15 min at room temperature.

Table I. Material information for cell setup.

#	Set up description	Material information	Manufacturer
1	Commercial CCM with high loadings	Nafion 115, 1 mg cm^{-2} Pt/C, 2 mg cm^{-2} Ir	Hiat gGmbh
2	Commercial CCM with low loadings	Nafion 115, 0.5 mg cm^{-2} Pt/C, 0.5 mg cm^{-2} Ir	Hiat gGmbh
3	Uncoated membrane and 2 GDEs	Nafion 115, E-TEK Black-Dry 0.5 mg cm^{-2} Pt/C	Hiat gGmbh and De Nora
4	Half coated membrane (A) and Pt-free GDE (C)	Nafion 115, 2 mg cm^{-2} Ir, N-doped CNT GDE, 1.5 mg cm^{-2}	Hiat gGmbh and synthesized as in Ref. 18
5	Half coated membrane (C) and Pt-free GDE (A)	Nafion 115, 1 mg cm^{-2} Pt, N-doped CNT GDE, 1.5 mg cm^{-2}	Hiat gGmbh and synthesized as in Ref. 18

Afterward, the titanium PTLs are impregnated with 10 μl of Nafion^{TM}-solution from both sides, dried for 15 min, then 10 μl of Nafion^{TM}-solution from both sides is reapplied and again dried for 15 min. The solution is a commercial mixture of 5 wt% Nafion^{TM} in lower aliphatic alcohols and water contains 15%–20% water from Sigma Aldrich. A typical PTL impregnation process can be seen in Fig. 2a seconds after application of 10 μl and (b) after 2 min of waiting time. A similar procedure is used for the cathode carbon PTLs and carbon GDEs with only 5 μl. The amount of electrolyte was adjusted according to the thickness of the layer.

Measurement protocol.—Here, the measurement protocol for testing is described. The cell is assembled in a wet state. The CCMs, as received from the manufacturer, are immersed in DI water for one hour at room temperature to ensure full humidification. After assembling the cell, it is inserted into an E40 test station from Greenlight Innovation. Anode water recirculation at 60 °C with a flow rate of 80 ml min^{-1} is used. Thermal conditioning is carried out by running the water recirculation for 30 min with an unpolarized cell. Afterward, the cell is compressed to 3 kN. Then, polarization measurement at ambient pressure conditions is started. Polarization behavior is assessed by galvanostatic step profile with current steps between 0.005 and 2 A cm^{-2} with impedance measurements at every current density step for determining high-frequency resistance R_{HF}. A frequency range of 100 kHz to 0.1 kHz with 11 points per decade is used. The polarization measurement is carried out thrice.

Potential distributions with RE on both electrodes.—The measured full cell voltage includes: (i) U_{rev} - reversible cell voltage and the voltage loss sources, (ii) R^{mem} - Membrane resistance for proton transport, (iii) R_{el} - electronic resistance of cell parts including contact resistances, (iv) R_{H+} - proton resistances of anode and cathode catalyst layer (v) η_{act} - kinetic losses (vi) η_{mt} - mass transport losses as can be seen in Eq. 1.

$$U_{cell} = U_{rev} + \eta_{act} + i(R^{mem} + R_{el} + R^{cl}_{H+}) + \eta_{mt} \quad [1]$$

The cell voltage can be further decomposed into the anode and cathode contributions (Eq. 2).

$$\begin{aligned} U_{cell} = {} & E^{A} - E^{C} + \eta^{A}_{act} - \eta^{C}_{act} \\ & + i(R^{ptl,A}_{el} + R^{ptl|cl,A}_{el} + R^{cl,A}_{H+} + R^{cl,A}_{el} + R^{mem}_{H+} \\ & + R^{cl,C}_{el} + R^{cl,C}_{H+} + R^{ptl|cl,C}_{el} + R^{ptl,C}_{el}) + \eta^{A}_{mt} + \eta^{C}_{mt} \end{aligned} \quad [2]$$

All three main loss contributions (kinetic losses, mass transport losses, and ohmic losses) occur on both anode and cathode. Kinetic and mass transport losses are indicated as $\eta_{act}{}^{A}$, $\eta_{mt}{}^{A}$, $\eta_{act}{}^{C}$, $\eta_{mt}{}^{C}$ for both electrodes, respectively. For the ohmic losses, the proton resistance in the catalyst layers and the electronic resistance in both the catalyst layers and the PTLs are decomposed into $R_{el}{}^{ptl,A}$, $R_{el}{}^{cl,A}$, $R_{H+}{}^{cl,A}$, $R_{el}{}^{ptl,C}$, $R_{el}{}^{cl,C}$, $R_{H+}{}^{cl,C}$. In addition to the electronic resistances of the components, resistances at the interfaces can occur, both on anode and cathode ($R^{ptl|cl,A}$ and $R^{ptl|cl,C}$). However, these single losses cannot be determined from only full cell measurements. Therefore, RE measurements are required. Their working principle will be described subsequently.

SBRE on the anode.—The SBRE gives access to the CL proton potential at the electrode where it is located. This is sketched in Fig. 3. From right to left, the electric potential $\Phi_{electric}$ at the cathode increases throughout the carbon PTL due to its electronic resistance. Moreover, the interface of the PTL to the cathode CL has an electronic contact resistance. In the CL, another increase occurs due to electronic resistance of the CL. The difference between electric and ionic potential Φ_{ionic} represents the equilibrium potential of the hydrogen evolution reaction (HER) based on the Nernst equation and the kinetic overpotential and mass transport losses. Subsequently, we follow the proton potential. Due to ionic resistances, the proton potential increases throughout the CL. The membrane's resistance leads to another increase in ionic potential. Like the cathode, the anode CL has a protonic and electronic resistance. The half-cell potential of the oxygen evolution reaction (OER), the kinetic overpotential of the OER, and mass transport losses account for the difference between the electric and protonic potential. The behavior in the PTL and the interface between CL and PTL are similar to the cathode PTL. Finally, the electric potential at the anode PTL against the electric potential at the cathode PTL equals the cell voltage. The measured voltage would be slightly higher in an actual setup due to electronic and contact resistance in the bipolar plates. These have been omitted for the sake of simplicity.

Here the SBRE probes to the proton potential of the CL at the interface to the PTL, this is realized through the impregnation of the PTL with Nafion^{TM} as described in materials section.

With the SBRE, the following two voltage measurements between the RE and the electric potential of the anode and cathode, in addition to the full cell voltage U_{cell} measurement, can now be provided (Eqs. 3 and 4):

$$U_{A-RE_A} = E^{A} + \eta^{A}_{act} + i(R^{ptl,A}_{el} + R^{ptl|cl,A}_{el}) + \eta^{A}_{mt} \quad [3]$$

$$\begin{aligned} U_{C-RE_A} = {} & E^{C} + \eta^{C}_{act} - \eta^{C}_{mt} \\ & - i(R^{cl,A}_{H+} + R^{cl,A}_{el} + R^{mem}_{H+} + R^{cl,C}_{el} + R^{cl,C}_{H+} + R^{ptl|cl,C}_{el} + R^{ptl,C}_{el}) \end{aligned} \quad [4]$$

Contributions in the measured voltages for RE to anode (Eq. 3) include the OER half-cell potential (E^{A}), anode activation overpotential ($\eta^{A}{}_{act}$), contact resistance anode CL to PTL ($R^{ptl|cl,A}{}_{el}$), and PTL electric resistance ($R^{ptl,A}{}_{el}$). For RE to cathode (Eq. 4), the voltage includes HER half-cell potential (E^{C}), cathode activation overpotential ($\eta^{C}{}_{act}$), contact resistance cathode CL to PTL ($R^{ptl|cl,C}{}_{el}$), PTL electronic resistance ($R^{ptl,C}{}_{el}$), ionic and electronic resistances in CLs ($R^{cl,A}{}_{el}$, $R^{cl,C}{}_{el}$, $R^{cl,A}{}_{H+}$, $R^{cl,C}{}_{H+}$), ionic resistance in membrane $R^{mem}{}_{H+}$ and mass transport loss ($\eta^{C}{}_{mt}$).

SBRE on the cathode.—The SBRE can be located on either anode or cathode side. For the cathode side, the sketch from Fig. 3 is modified regarding the RE access potential in Fig. 4. The measured potentials are indicated from RE to cathode and from RE to anode.

For a detailed description of the potential distributions we refer to the previous paragraph. The contributions to the measured voltages between the RE and both half-cells are given in Eqs. 5 and 6.

$$\begin{aligned} U_{A-RE_C} = {} & E^{A} + \eta^{A}_{act} + \eta_{mt}{}^{C} \\ & + i(R^{ptl,A}_{el} + R^{ptl|cl,A}_{el} + R^{cl,A}_{H+} + R^{cl,A}_{el} + R^{mem}_{H+} + R^{cl,C}_{el} + R^{cl,C}_{H+}) \end{aligned} \quad [5]$$

$$U_{C-RE_C} = E^{C} + \eta^{C}_{act} + i(R^{ptl|cl,C}_{el} + R^{ptl,C}_{el}) - \eta^{C}_{mt} \quad [6]$$

Concluding remarks on setup.—Coming back to the introduction, the SBRE enables the measurement of the potential differences between the half-cells (anode, cathode) towards the RE. Within these voltages, the kinetic overpotentials from each electrode are included. With an interference-free setup, especially local EIS measurements, it makes no difference on which side the SBRE is placed since, in all cases, the different losses are split up and can be determined separately. However, in an actual setup with measurement issues, the best practice tip is to place the RE close to the electrode of interest. The reason is that the measured voltage includes only a few additional losses, which are the electronic resistance of PTL and contact resistance to CL. These are considered small since the membrane's proton transport is the leading cause of ohmic losses.[19] In other words, depending on the side where the SBRE is located,

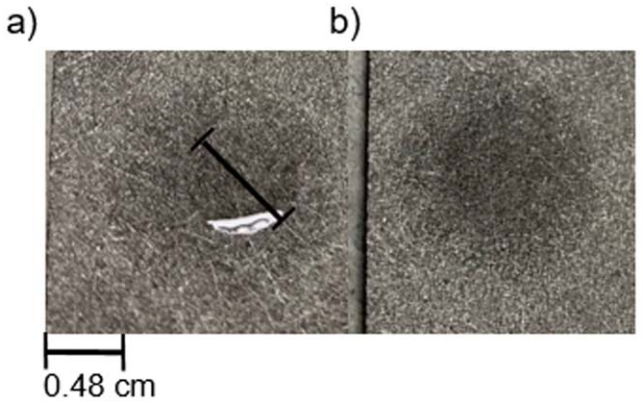

Figure 2. Nafion™ impregnation in titanium PTLs, (a) directly after impregnation and (b) after 2 min.

the measured voltage includes a small part of the electronic resistances Eq. 3 (anode) and 6 (cathode) or a large part of electric and ohmic resistances as in Eqs. 4 and 5. which all together form the HFR as shown in Eq. 7.

$$R_{\mathrm{HFR}} = R_{\mathrm{el}}^{\mathrm{ptl|A}} + R_{\mathrm{el}}^{\mathrm{ptl,A}} + R_{\mathrm{el}}^{\mathrm{ptl|C}} + R_{\mathrm{el}}^{\mathrm{ptl,C}} + R^{\mathrm{mem}} + R_{\mathrm{H+}}^{\mathrm{a}} + R_{\mathrm{H+}}^{\mathrm{c}} \quad [7]$$

It should be pointed out that the proton conduction resistance in the catalyst layer mentioned here describes the part that accounts for the migration of protons to the membrane at the anode side (R^{a}_{H+}) and to the catalyst particles at the cathode side (R^{c}_{H+}). It does not refer to the resistance in the RC circuit parallel to the double layer capacitance in a typical electric equivalent circuit (which represents the activation losses).

Data evaluation: HFR and Tafel analysis.— *Data evaluation for full cell measurements.*—The HFR is measured via electrochemical impedance spectroscopy (EIS) in the full cell. It is assumed that the ohmic cell resistance equals the measured high-frequency impedance, where the imaginary part of the impedance equals zero. In this work, it is calculated by linear interpolation of data at the intercept with the x-axis ($-\mathrm{Im} = 0$) in the Nyquist plot. Data from polarization measurements and HFR measurements is used to calculate the HFR corrected voltage (Eq. 8).

$$U_{\mathrm{iR_{HFfree}}} = U_{\mathrm{cell}} - i\,R_{\mathrm{HF}} \quad [8]$$

The HFR-corrected voltage is required for a Tafel analysis. For the full cell, the Tafel analysis in this work is carried out via linear interpolation of the HFR corrected voltage in a logarithmic current density region of 0.01–0.1 A cm^{-2}. This is described in Eq. 9 where the kinetic overpotential η_{act} is equal to the difference between $U_{\mathrm{iR_{HFfree}}}$ and the reversible full cell voltage U_{rev}, b is the Tafel slope, and i_0 [A $\mathrm{cm_{geo}}^{-2}$] is the apparent exchange current density.

$$\eta_{\mathrm{act}} = b\,\log\left(\frac{i}{i_0}\right) \quad [9]$$

If EIS is carried out via RE measurement, it can theoretically give information about the ohmic resistance of the half-cell. Ideally, this half-cell resistance is used to calculate the HFR-corrected half-cell voltage.

The Tafel approximation is justified for large overpotentials. It should be noted that a linear approximation is another frequently used simplification of the Butler-Volmer equation, valid for small kinetic overpotentials. The kinetic overpotential follows the current density linearly as in Eq. 10 where α_{f} is the transfer coefficient for the forward reaction (e.g. HER) and α_{b} for the backward (e.g. hydrogen oxidation reaction).

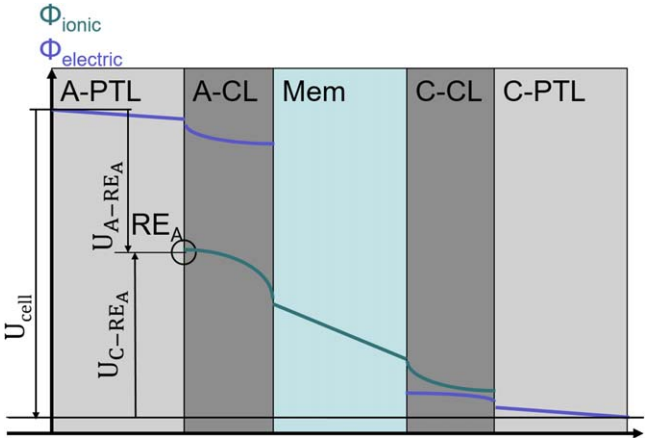

Figure 3. Electric and protonic potential distribution in a typical 5-layer PEM water electrolysis cell, RE located at anode electrode, indication of potential measurements.

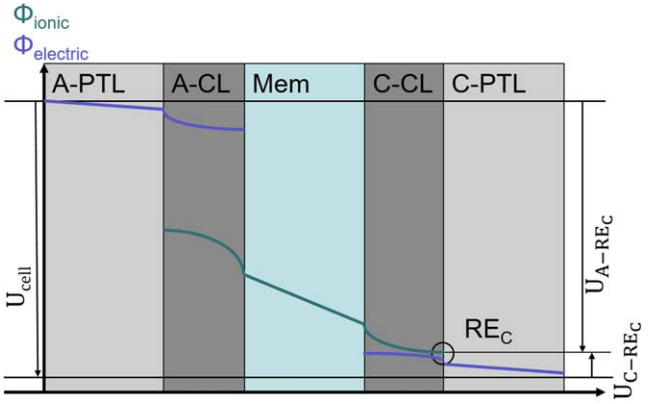

Figure 4. Proton and electron potential distribution in a typical 5-layer PEM water electrolysis cell, RE situated at cathode electrode, indication of voltage measurements.

$$\eta_{\mathrm{act}} = \frac{i}{i_0}\,\frac{R\,T}{F(\alpha_{\mathrm{f}} + \alpha_{\mathrm{b}})} \quad [10]$$

In the current work, Tafel approximation is used for all kinetic analyses. The aim is to gain a set of parameters for comparison. However, the HER usually is a fast reaction and thus protrudes in the range of linear approximation. Therefore, additional linear regression is carried out with HER data in the SI. The sum of the transfer coefficients α_{f} and α_{b} can be assumed to equal one.[20]

Data evaluation for RE measurements.—In this work, the half-cell resistance measurement via EIS is not implemented. For the half-cell Tafel analysis, the following assumption is made. At the low current density region (0.01–0.1 A cm^{-2}) and due to the small electronic resistance of the PTL and the contact resistance of PTL to CL, no correction is carried out on the half-cell voltage for kinetic analysis when locating the SBRE at the electrode of interest. In other words, the measured values are assumed to represent $E^{\mathrm{c}}+\eta^{\mathrm{c}}_{\mathrm{act}}$ when measuring at the cathode side towards the cathode electrode and $E^{\mathrm{a}}+\eta^{\mathrm{a}}_{\mathrm{act}}$ when measuring at the anode side towards the anode electrode. In the case of measuring at the opposite side, the resistance is assumed to be close to the full cell resistance and the correction is carried out with the cell HFR. The Nernst potential for both electrodes is calculated via the following equations (Eqs. 11 and 12). Tafel fitting for the half-cells is carried out as

described in Eq. 9.

$$E^{C} = 0\ \mathrm{V} + \frac{RT}{2F} ln\left(\frac{c_{H_2}^{ref}}{c_{H_2}}\right) \quad [11]$$

$$E^{A} = \frac{\Delta G^0}{2F} + \frac{RT}{2F} ln\left(\sqrt{\frac{c_{dsg,O_2}}{c_{dsg,O_2}^{ref}}}\right) \quad [12]$$

Results and Discussion

Since the ionic connection is crucial for SBRE, it is analyzed, and the proton transport is proven for the Nafion™ impregnated PTLs. Once the proton bridge through the PTL is guaranteed, the three-electrode measurements can be carried out. Therefore, the voltages of the full cell and half-cells as a function of current density for standard materials and the RE on both sides are presented. Last, a focus on kinetic analysis is made.

Ionic connection.—Establishing the ionic connection of the SBRE towards the electrode, done here by impregnating the PTL with Nafion™, results in a trade-off between proton conductivity through the PTL and additional mass transport losses due to covered pores. This subchapter thoroughly studies impregnation and its effects. Analysis has been carried out for titanium and carbon PTL and will be subsequently explained for the example of a titanium PTL. The first step to assure the presence of Nafion™ in some of the pores of the PTL is an analysis via scanning electron microscopy (SEM) with energy dispersive X-ray analysis (EDX). The analysis is carried out for the titanium PTL used at the anode side. The carbon-PTL from the cathode side is thinner and causes fewer issues regarding proton transport. The carbon PTL impregnation has also been briefly explained elsewhere,[7] while the titanium PTL impregnation is novel.

The result of an impregnated PTL is shown in Fig. 5 (top view). Nafion™ contains, among others, the element fluorine.[3] The element-specific plot of the fluorine (40.0 mass%) distribution shows that fluorine can be observed on all the titanium fibers (46.8 mass%), and signals are concentrated on the flanks of the titanium fibers. The remaining fractions are divided into carbon (10.2 mass%), iridium (2.8 mass%), and sulfur (0.2 mass%).

Once the presence of Nafion™ is assured, its functionality as a proton carrier is analyzed. This electrochemical proof is carried out through a hydrogen pump experiment, with a setup shown in Fig. 6. In this setup, an impregnated PTL is located between two Nafion™ membranes. One membrane is smaller than the PTL to ensure the membranes do not touch. On each side, a carbon GDE with Pt coating is located. Materials correspond to #3 in Table I. The sandwich is placed in a regular electrolysis cell manufactured by Fraunhofer ISE and one side is flushed with hydrogen at a pressure of 2 bar while the other has water circulation. A compression of 2 kN is applied. A voltage of 1 V is set to the cell and the current is measured. The current scales with the number of hydrogen ions passing through the two membranes and the impregnated PTL in the middle.

A PTL with low impregnation of 10 μl is compared to a highly impregnated PTL (100 μl). The former results in a current of 11 mA, while the highly impregnated PTL results in a current of 300 mA. Based on the measured values, it can be shown that the amount of Nafion™ significantly influences the ionic conductivity of the PTL.

After showing the need for an impregnation, its effect on cell performance is analyzed. Electrolysis tests were performed with untreated PTL and PTL with Nafion™ impregnation combined, in both cases, with low loading CCMs (#2 in Table I). The impregnation procedure corresponds to the one described in material and methods section.

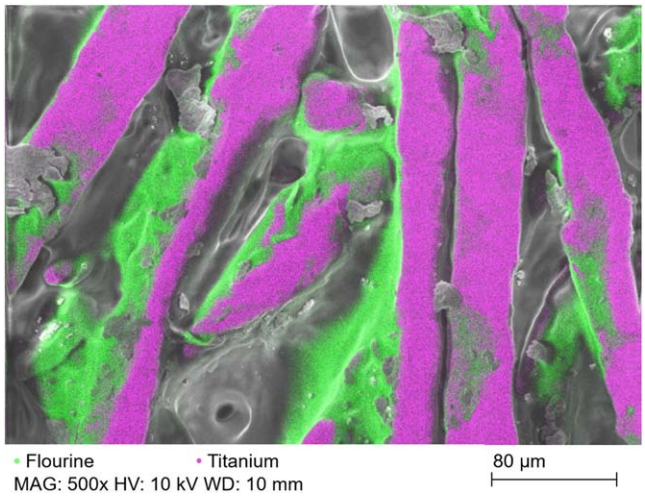

Figure 5. EDX-Map of a top view of a Nafion™- impregnated Titanium PTL, fluorine marked in green and titanium marked in purple.

The results are shown in Fig. 7a. The impregnated PTL results in a lower performance compared to the standard PTL. However, the performance at low current densities, which are the most interesting for later kinetic analysis, do not differ significantly.

A more detailed analysis of the kinetic region for the standard PTL results in a Tafel slope of 51 mV dec^{-1}, 95% CI [47, 54], and an exchange current densities of $5.52{\cdot}10^{-8}$ A cm^{-2}, 95% CI [$2.16{\cdot}10^{-8}$, $1.41{\cdot}10^{-7}$]. The values for the impregnated PTL lie with 49 mV dec^{-1}, 95% CI [47, 52] and $4.07{\cdot}10^{-8}$ A cm^{-2}, 95% CI [$1.93{\cdot}10^{-8}$, $8.60{\cdot}10^{-8}$] close by. The kinetic region seems to be mostly unaffected by the impregnation.

Figure 7b shows that the differentiation of the cell voltage arises mostly from the difference in the HFR, which is significantly higher for the impregnated sample. The impregnation apparently influences the electric resistance, covering the fibers with Nafion™. Furthermore, mass transport issues need to be managed. Figure 7c underlines an increase at current densities larger than 1.5 A cm^{-2} for the impregnated PTL.

Consequently, the SBRE measurements will focus on the current density range from 5 mA cm^{-2} to 0.1 A cm^{-2} However, since the application of the SBRE is also desired for large current densities and should influence the cell performance, the impregnation leaves room for optimization.

At this point, a successful Nafion™ impregnation can be reported. Fluorine (and therefore Nafion™) is mainly present along the fibers. The cell's performance is, unfortunately, affected but only at high current densities. However, data is suitable for kinetic analysis. Reducing negative influence at high current densities remains a challenge for future investigations.

Measured full cell and half-cell voltages over current density.—Since locating a SBRE at the impregnated anode PTL is novel, this setup will be discussed first. Afterward, the data for the SBRE at the cathode will be presented. This subchapter aims to give an overview of the information that can be accessed with a SBRE.

Reference electrode at anode.—In Fig. 8a the measured voltages for full cell and half-cells are plotted over current density. Material for this data corresponds to #1 in Table I. The full cell signal (black) starts at a voltage of about 1.4 V and increases over current density to around 1.9 V, as expected for a PEMWE cell. Additional information on the half-cell data is added, namely the voltage signals between the RE on the anode side towards the anode (A-RE$_A$) and cathode (C-RE$_A$). The anode to reference electrode signal (U_{A-RE_A}) includes contributions stated in Eq. 3. Since the OER half-cell potential (E^A) and the anode activation overpotential (η^A_{act})

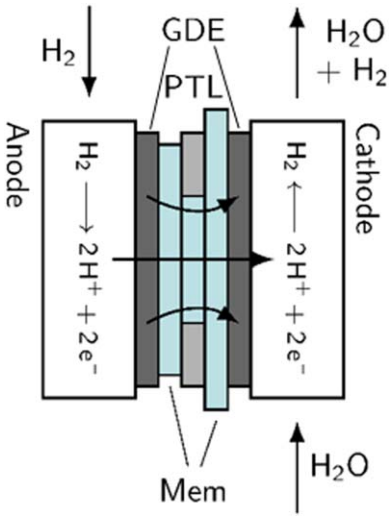

Figure 6. Sketch of the experimental setup for ionic conductivity testing of impregnated PTL via hydrogen pump.

are part of it, the signal for current densities towards zero starts in the same range as the full cell voltage signal. However, contributions from ohmic losses are negligible (membrane is not included in the A-RE$_A$ signal), and the increase with current density is less pronounced. Different U_{C-RE_A}, which can be seen in the Eq. 4. The corresponding C-RE signal in Fig. 8a is negative, since the reference electrode potential is higher than the cathode electrode potential. The signal starts roughly at the origin and decreases over current density. This is due to the increasing ohmic, mass transport, and kinetic losses. The difference of both half-cell signals results in the full cell voltage measurement ($U_{cell} = U_{A-RE_A} - U_{C-RE_A}$). The temperature in the RE solution is room temperature, around 20 °C, and thus the Ag/AgCl RE potential is 0.191 V vs NHE. Measured values are corrected to potential vs SHE with this value.

Figure 8b shows the full cell HFR from EIS measurement. The HFR is around 200 mΩ cm^2. Due to an unsteady signal in the impedance spectrum at current densities lower than 1 A cm^{-2}, the median HFR of all values higher than 1 A cm^{-2} is used. A dashed line connects the corresponding points. As mentioned earlier, a separately measured HFR for anode and cathode would be valuable additional information for the RE implementation but has not been implemented until now.

Figure 8c presents the iR_{HF}-corrected cell voltage, which is used for the Tafel analysis of the full cell as explained in Eq. 9. The values attained here are a Tafel slope of 51 mV dec^{-1}, 95% CI [47, 55], and an exchange current density of $2.66{\cdot}10^{-7}$ A cm^{-2}, 95% CI [$1.04{\cdot}10^{-7}$, $6.79{\cdot}10^{-7}$]. Tafel slope and exchange current density lie in a reasonable range. Previous work with similar setups measured Tafel slopes in the ranges of 42 to 44 mV dec^{-1}[21] and 50 to 60 mV dec^{-1}.[18] Exchange current densities lay in the range of 1.6 to $2.3{\cdot}10^{-8}$ A cm^{-2} in these works.[21] Further literature reports values for Tafel slope of 38.9 mV dec^{-1}[22] to 81 mV dec^{-1}[19] and exchange current density of $1.5{\cdot}10^{-3}$ A cm^{-2} to $1{\cdot}10^{-12}$ A cm^{-2}[23] for PEMEL cell.

Reference electrode at cathode.—After showing the results for the SBRE at the anode, data for the RE connected to the cathode is presented in Fig. 9. The temperature in the RE solution increased over time due to heat sources in the vicinity of the beaker. A temperature of 40 °C is assumed; thus, the Ag/AgCl RE potential is 0.211 V vs NHE. Similar to Fig. 8a, the cell voltage increases from around 1.4 V to 1.9 V over current density. However, the half-cell signals are different due to the change in location of the SBRE. If the RE is located at the cathode, the signals include the contributions as in Eqs. 5 and 6. In other words, when placed close to the cathode and measuring towards the cathode, the signal only includes HER kinetics, small ohmic losses, and mass transport losses from the cathode electrode. The HER kinetics are fast and the electronic resistances are small compared to ionic resistances.[5] These result in a slight decrease of the measured voltage (U_{C-RE_C}) over current density. In contrast, the voltage increase between anode and RE (U_{A-RE_C}) is larger since it contains the major part of the ohmic losses in addition to OER overpotential and mass transport losses. The HFR values around 180 mΩ cm^2 shown in Fig. 9b as well as the Tafel slope and the exchange current density, being 48 mV dec^{-1}, 95% CI [46, 51] for Tafel slope and $1.17{\cdot}10^{-7}$ A cm^{-2}, 95% CI [$6.75{\cdot}10^{-8}$, $2.05{\cdot}10^{-7}$], in Fig. 9c are in a close range as for the case with the RE at the anode (Fig. 8). This is as expected since the same materials are used.

As an interim conclusion, the SBRE works on both anode and cathode sides and provides supplemental data in addition to the full cell voltage. Moreover, HFR and Tafel slope of the full cell measurement can still be assessed. In the following subchapter, the analysis of the additional half-cell data is shown.

Analysis of half-cell potentials.—*Analysis of the OER kinetics.*—This subsection deals with a kinetic analysis for the half-cell voltages. First, the anode kinetics where the sluggish OER takes place is analyzed. Data shown in Fig. 8 is used with the RE being located at the anode. The signal U_{A-RE_A} has minimal influence of additional loss mechanisms and is directly employed for Tafel analysis. The results can be seen in Fig. 10. For calculating i_0 from the measured data, the half-cell Nernst potentials need to be calculated as shown in Eq. 12.

The Tafel slope for the OER is calculated to be 46 mV dec^{-1}, 95% CI [45, 47], slightly lower than the full cell Tafel slope of around 51 mV dec^{-1}. Tafel slope and exchange current density

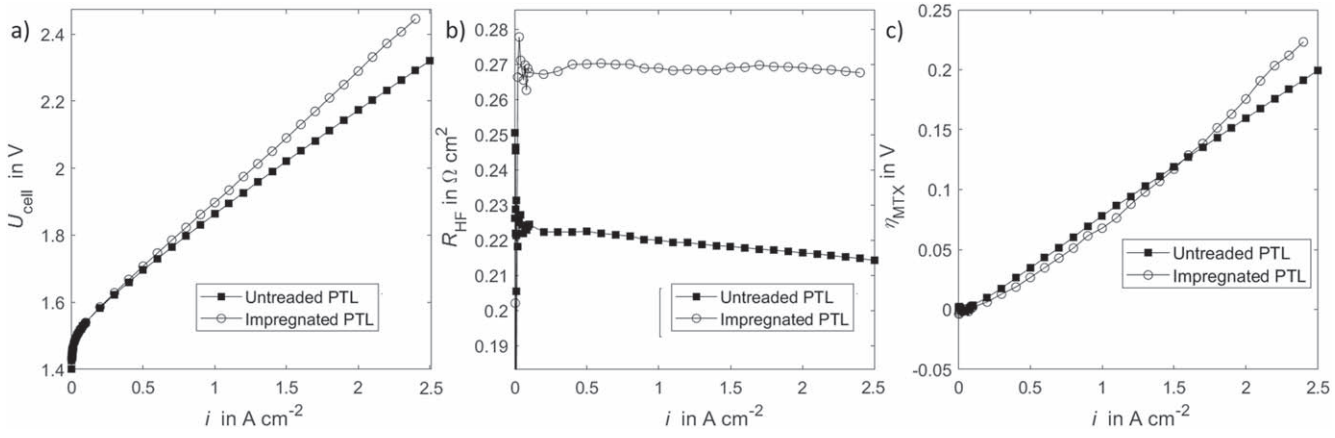

Figure 7. (a) Cell polarization curve, (b) HFR and (c) Mass transport losses of untreated and impregnated PTL at 60 °C and ambient pressure.

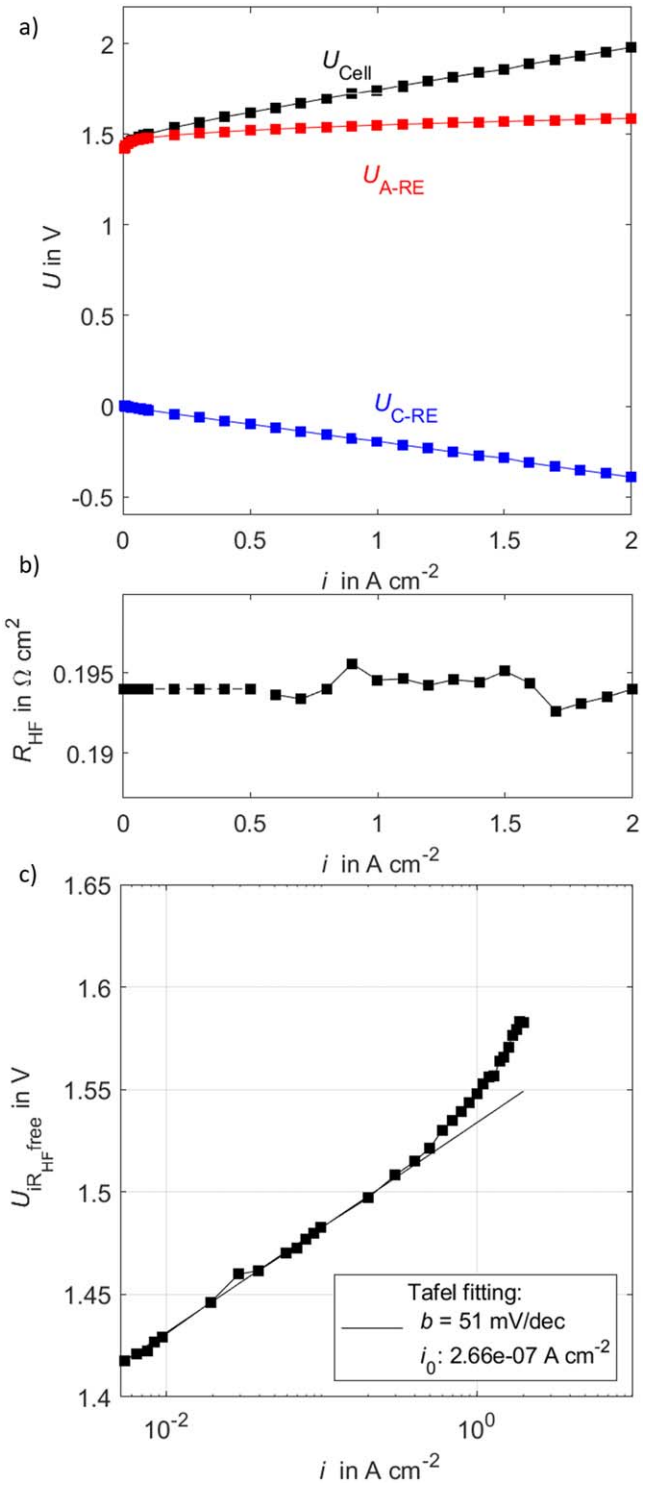

Figure 8. Cell voltage analysis of a PEM water electrolysis cell with standard material at 60 °C with RE at anode. (a) Polarization curves, (b) HFR over current density, (c) HFR corrected polarization curve over logarithmic current density.

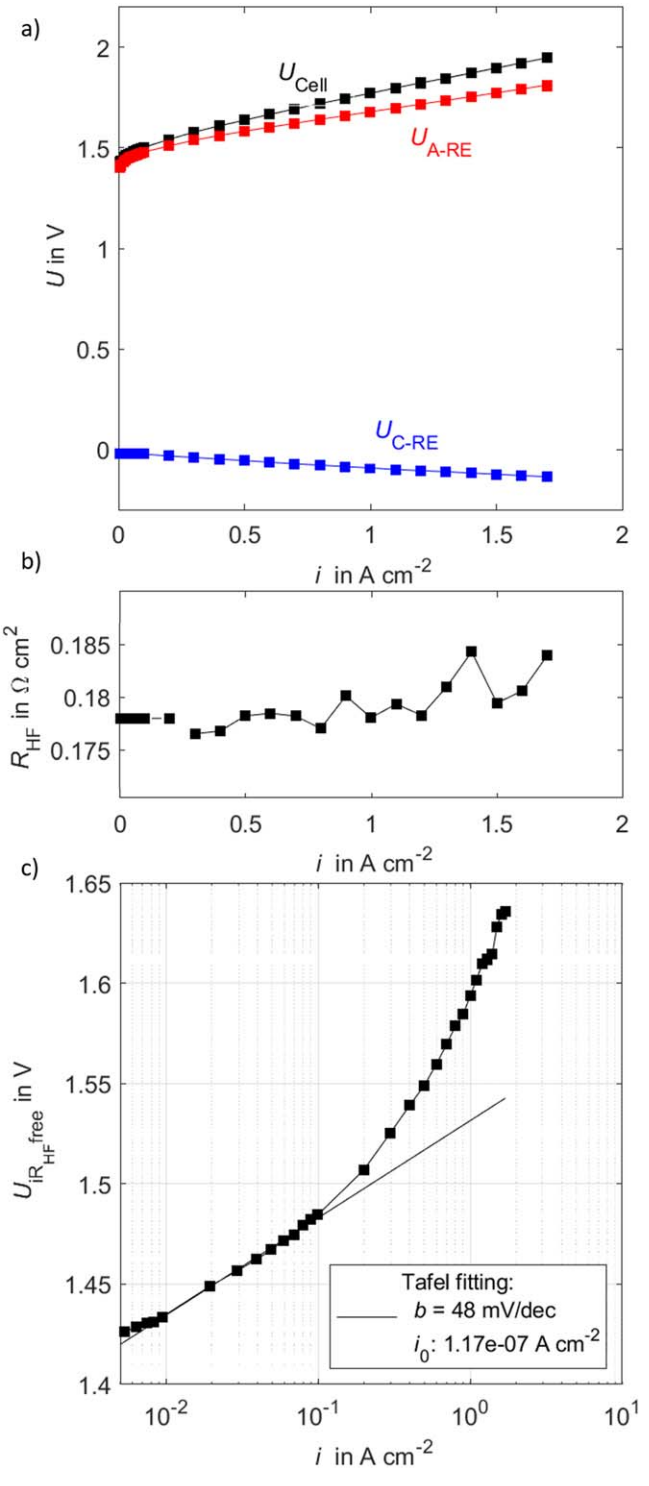

Figure 9. Cell voltage analysis of a PEM water electrolysis cell with standard material at 60 °C with RE at cathode: (a) Polarization curves, (b) HFR over current density, (c) HFR corrected polarization curve over logarithmic current density.

($1{\cdot}10^{-7}$ A cm^{-2}, 95% CI [$8.36{\cdot}10^{-8}$, $1.21{\cdot}10^{-7}$]) lie in a reasonable range. Tafel slope for OER with iridium catalyst in rotating disc electrode (RDE) setups was found to be 50–60 mV dec^{-1}.[24] Recent work from Lazaridis et al. stated that OER catalyst activities derived from liquid electrolyte cells and thin-film electrodes reliably match MEA-obtained values.[25] The results highlight the benefit of using a RE since the OER kinetics can now be estimated apart from the HER. This has not been carried out with a SBRE so far. However, some losses, such as mass transport and ohmic losses, are included in the measured signal and could influence the Tafel analysis, which is most probably small, especially at low current densities. Ideally, the intended half-cell HFR measurement would yield the exact loss contribution so that the signal could be corrected. Hitherto, this is not possible due to inconclusive EIS half-cell spectra. Corresponding Nyquist plots can be seen in the SI.

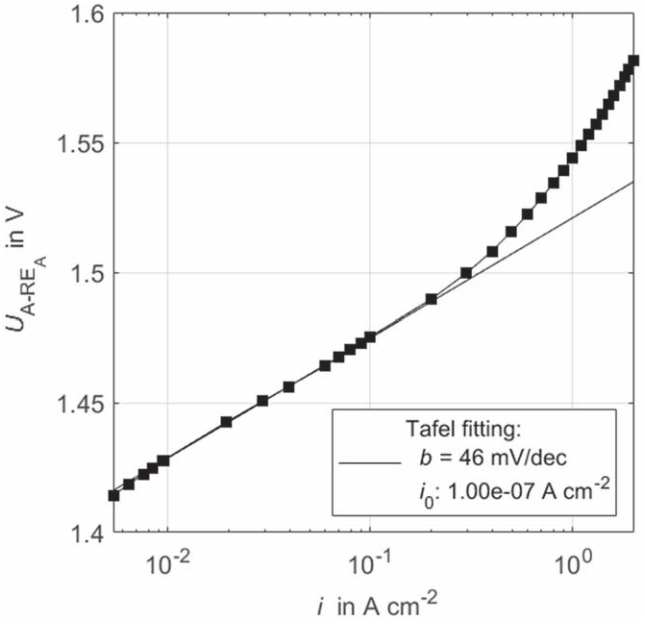

Figure 10. OER Tafel analysis of A-RE_A, signal with RE at anode.

The anode Tafel analysis can also be carried out when the SBRE is placed at the cathode. However, ionic and electronic losses play a major role in the measured voltage signal in this case. Due to the yet unknown HFR shares, the full cell HFR is used to correct the measurement as a first assumption to filter the anode kinetic overpotential. The Tafel analysis for the OER reaction with a RE at the cathode can be seen in Fig. 11. Data for calculation is the one shown in Fig. 9.

The calculated Tafel slope of 45 mV dec^{-1}, 95% CI [44, 46], in Fig. 11 is very close to the one measured with the RE at the anode, the CI overlap. The same applies to the exchange current density of $7.03{\cdot}10^{-8}$ A cm^{-2}, 95% CI [$5.63{\cdot}10^{-8}$, $8.77{\cdot}10^{-8}$]. Not only can it be shown that the kinetics of both electrodes can be analyzed separately, but the placement of the SBRE results in matching graphs. If the signal is not corrected by the influence of ohmic resistances, it leads to a deviation of the Tafel slope. In Fig. 11, the signal is corrected by the full cell HFR. For high current densities, the measured voltage lies below the Tafel line. This indicates that the actual half-cell HFR is smaller than the applied full cell HFR. However, the assumption works well for low current densities. This underlines the importance of correcting the measured data with additional ionic and electronic losses. Again, ideally, the exact half-cell HFR value would be used for the correction, but it is not yet available.

Analysis of HER kinetics.—After the anode data is studied through the additional signal from the RE, a detailed analysis of the cathode data is carried out. First, we show in Fig. 13 the Tafel analysis of the cathode to RE signal when the SBRE is placed at the cathode.

In contrast to the OER kinetics, the HER kinetics show a small Tafel slope, as seen in Fig. 12. The Tafel slope is −3 mV dec^{-1}, 95% CI [−5, −1], corresponding to a fast reaction and resulting in more minor losses. The exchange current density is also significantly higher compared to OER, attending $6.44{\cdot}10^{-4}$ A cm^{-2}, 95% CI [$5.9{\cdot}10^{-5}$, $7.0{\cdot}10^{-3}$]. Results for linear approximation can be found in the SI.

The results highlight the additional value from using a RE since the HER kinetics can now be estimated apart from the OER. This has not been carried out with a SBRE so far but could be relevant in the case of cathode catalyst degradation. However, some electronic losses are included in the measured signal and could influence the Tafel analysis. Since it is impossible to obtain reliable HER kinetic data for carbon-supported Pt catalysts from RDE measurements in acidic electrolyte,[25] literature data is not shown here.

Again, the RE can be placed on either anode or cathode side. Subsequently, the HER kinetic analysis is shown when data is collected with RE at the anode. In this case, the ionic and electronic losses play a significant role in the measured signal. As a first assumption, the full cell HFR is used to correct the measurement and filter the cathodic kinetic overpotential.

The Tafel slope lies in the same range as for the RE at the cathode, the CI overlap. Tafel slope is calculated to −5 mV dec^{-1}, 95% CI [−9, −1] and exchange current density to $3.3{\cdot}10^{-3}$ A cm^{-2}, 95% CI [$6.25{\cdot}10^{-4}$, $17.4{\cdot}10^{-3}$]. Results for linear approximation can be found in the SI. Again, the full cell HFR correction is valid for low current densities and results in incorrect values for higher current densities. The latter can be observed in Fig. 13 after 0.5 A cm^{-2}. For larger current densities, the HFR correction results in positive values. This is not correct and shows the limits of this approach. The real HFR for the C-RE signal is smaller than the cell HFR. However, the results at small current densities, where the Tafel analysis is typically done, agree with the theoretically expected values.

Interim conclusion.—The combined results of the full cell and half-cell kinetic analysis are summarized in Table II. As mentioned, the values lie in the same range independently of the RE location. Furthermore, as expected, the OER kinetics result in larger loss contributions than the HER.

As mentioned at the beginning, we recommend positioning the RE on the side to be investigated to reduce the signal's additional influences. Under the assumptions made, the kinetic analysis provides good results. In the future, it is expected that the half-cell impedance measurement can be included in the data analysis. The half-cell HFR values obtained from this will allow the RE to be placed regardless of the side of interest.

Additional applications for SBRE.—To this point, the SBRE setup has been demonstrated by analyzing anode and cathode kinetics separately. Now, two examples will be shown for possible use cases for which such an extended loss breakdown can be a beneficial analysis tool. For this, the electrodes are manipulated one after the other according to Table I #4 and #5.

Table II. Summary of experimental results from SBRE measurements on both sides.

SBRE location	Signal	Figure	Tafel slope *b* in mV dec^{-1}	Exchange current density i_0 in A cm^{-2}
@Anode	Full cell	Fig. 8	51	$2.66{\cdot}10^{-7}$
	A-RE	Fig. 10	46	$1.00{\cdot}10^{-7}$
	C-RE	Fig. 13	−5	$3.30{\cdot}10^{-3}$
@Cathode	Full cell	Fig. 9	49	$1.17{\cdot}10^{-7}$
	A-RE	Fig. 11	45	$7.03{\cdot}10^{-8}$
	C-RE	Fig. 12	−3	$6.44{\cdot}10^{-4}$

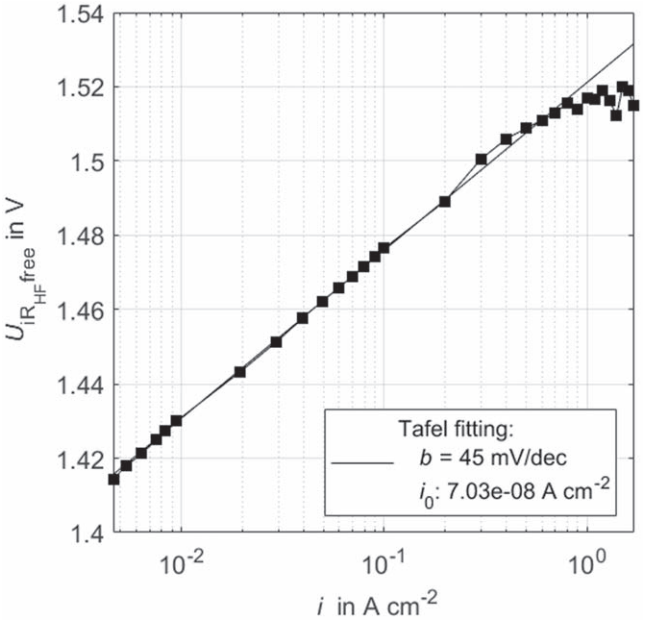

Figure 11. OER Tafel analysis of A-RE$_C$ signal with RE at cathode.

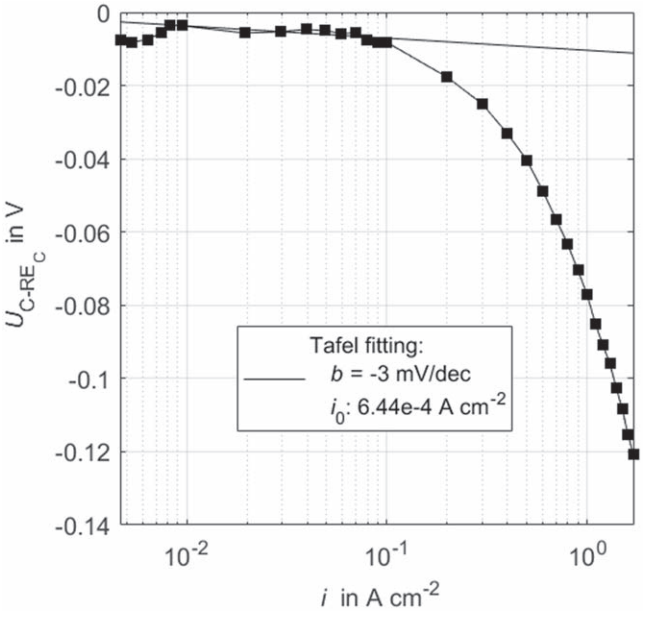

Figure 12. HER Tafel analysis with the C-RE$_C$ signal with RE at cathode.

Pt-free cathode catalyst.—Next, the SBRE setup is used to analyze a Pt-free catalyst on the cathode, which performs worse than the standard Pt/C catalysts. Materials for this experiment correspond to Table I #4. Figure 14a shows the cell and half-cell performances. The temperature of the external RE, connected to the anode side, was 20 °C and the potential 0.191 mV. While the setups with standard cathode catalyst (Pt/C) resulted in a voltage below 2 V at the largest current density (see Figs. 8 and 9), an increase up to above 2.5 V can be observed with the Pt-free catalyst, which fits previous experimental data.[18] Especially around a current density of 0.48 A cm^{-2} the full cell signal increases drastically. The distinct slope and the substantial increase of the cell voltage can be assigned entirely to the cathode (C-RE) signal, decreasing to −1 V at 1.8 A cm^{-2}. Meanwhile, the anode (A-RE) signal with standard Ir-black catalyst increases comparable to the previous measurements (Fig. 8a). Therefore, one can state that the RE

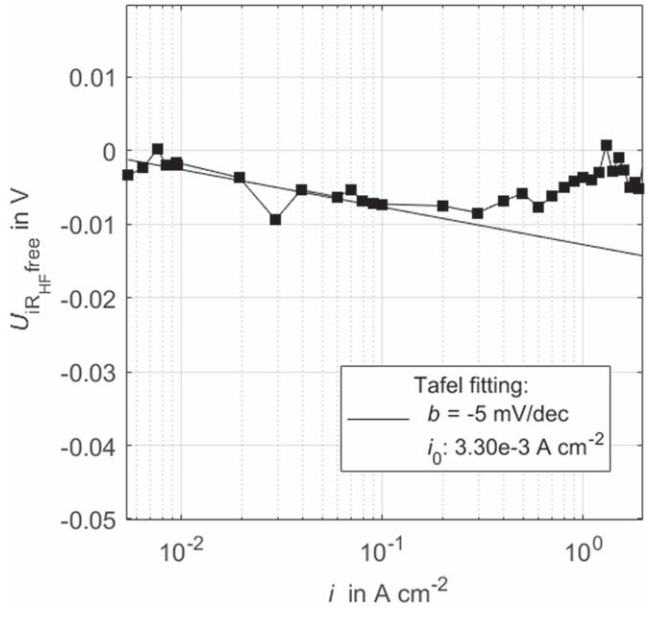

Figure 13. HER Tafel analysis of C-RE$_A$ signal with RE at anode.

enables the change in cell performance to be traced back to the cathode signal. The cell HFR, shown in Fig. 14b, increased slightly with the Pt-free catalyst material on the cathode. However, the measurement suffers from indistinct impedance spectra, especially at low current densities, which can most probably be attributed to the not optimized settings of the potentiostat to the varying resistances in the cell.

The Tafel analysis for this setup is shown in Fig. 15. While the OER Tafel analysis (Fig. 15b) is unaffected, the overall cell Tafel is significantly enlarged (Fig. 15a). Due to the Pt-free catalyst, the full cell Tafel slope reaches over 100 mV dec^{-1}. The SBRE allows tracking the cell deterioration back to the cathode CL (Fig. 15c). The HER Tafel slope is calculated to be −54 mV dec^{-1}, 95% CI [−63, −45]. It can be clearly shown that an additional value from RE is an experimental delimitation of the causes of general deterioration.

Unstable anode.—Finally, a low-performance, unstable anode made of platinum on carbon is used. Platinum is not only a worse OER catalyst compared to iridium, but the carbon support is also unstable at low pH and high potential in an oxygen environment. Materials correspond to #5 in Table I. Once again, the reference electrode is located at the anode side. The upper part of Fig. 16 shows the cell and A-RE voltage for beginning of test (BOT) corresponding to the first measurement and end of test (EOT). Between these two measurements, current density was ramped up from 0.005 A cm^{-2} to 0.1 A cm^{-2} within 500 s resulting in voltages of up to 2.4 V. The cell voltage at EOT is higher and increases steeper over current density. The same is valid for the $U_{A\text{-}RE}$ signal. The instability of the carbon anode results in a performance loss in the anode and thus cell voltage. However, the cathode to reference voltage signal, shown in Fig. 16 lower part, is mostly unaffected and stays in the same range. This example illustrates how a SBRE can trace the degradation in a system to one electrode or half-cell. Due to the low performance of the setup, Tafel analysis, as well as HFR measurements, result in values far from expectations and are not further analyzed. Compared to a standard setup, the $U_{C\text{-}RE}$ signal is slightly affected by the low-performing anode. This results in larger negative values in the lower part of Fig. 16 compared to standard materials. A possible reason can be a smaller effective active area due to the hindering of the OER reaction by the low performing anode CL.

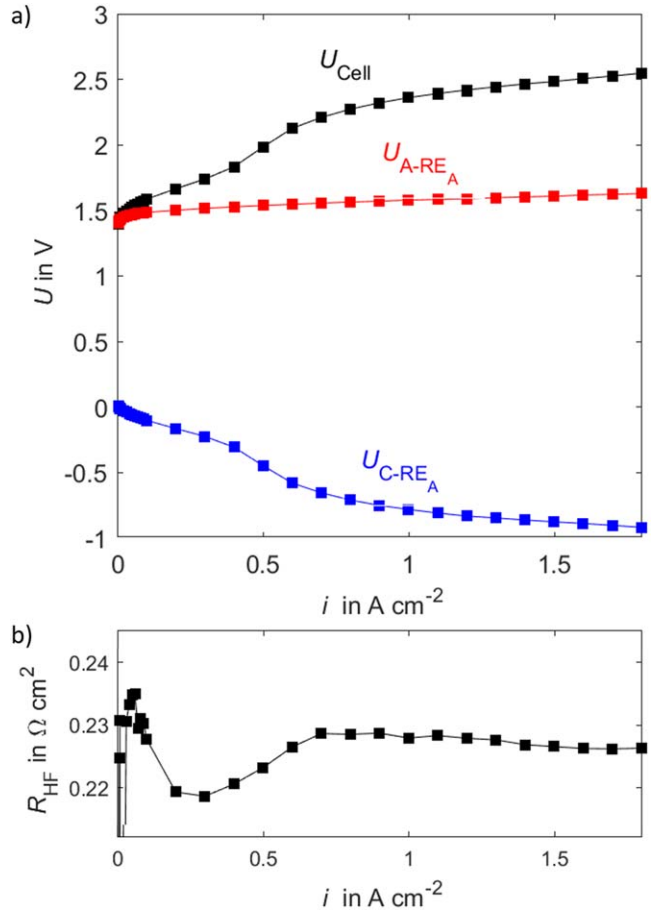

Figure 14. Measurement results for a low-performance cathode CL. (a) Polarization curves, (b) HFR over current density.

Summary and Conclusion

A SBRE setup for a water electrolysis test cell, including PTL impregnation, is presented. Experiments verify the functionality of SBRE. The measurements focus on the current density range from 5 mA cm^{-2} to 0.1 A cm^{-2}. At larger current densities, the trade-off between ionic connectivity and additional losses leaves room for the optimal amount of used electrolyte in the impregnation process. Additional analyses of half-cell kinetics are shown. At low current densities, for which HFR and mass transport losses are negligible, quantitative information about half-cell Tafel slope and exchange current density can be accessed. For the first time, OER and HER kinetic parameters are measured in a full cell setup. Tafel slope for OER attained values around 45 to 46 mV dec^{-1} and for HER −3 to 5 mV dec^{-1}. Exchange current density for OER and HER are calculated to be $0.7–1{\cdot}10^{-7}$ A cm^{-2} and $9.4–12.2{\cdot}10^{-3}$ A cm^{-2}, respectively. However, quantitative analysis (improvement of voltage loss breakdown) of the other electrochemical losses, especially at higher current densities, will only be possible when the half-cell HFR can be measured via EIS, which is the subject of ongoing research.

One of the reviewers contributed another consideration for future research. The external RE used in this work (Ag/AgCl) can leak silver and chloride ions into the system. Possible membrane contaminations have not interfered with the results in this work. However, alternative RE, such as a standard hydrogen RE, should be considered.

Additionally, two use cases of the SBRE are shown to detect the source of overall cell deterioration. When using a Pt-free cathode catalyst and a Pt/C catalyst on the anode, the full cell signal changes were successfully traced back to their respective origins. Thus, the

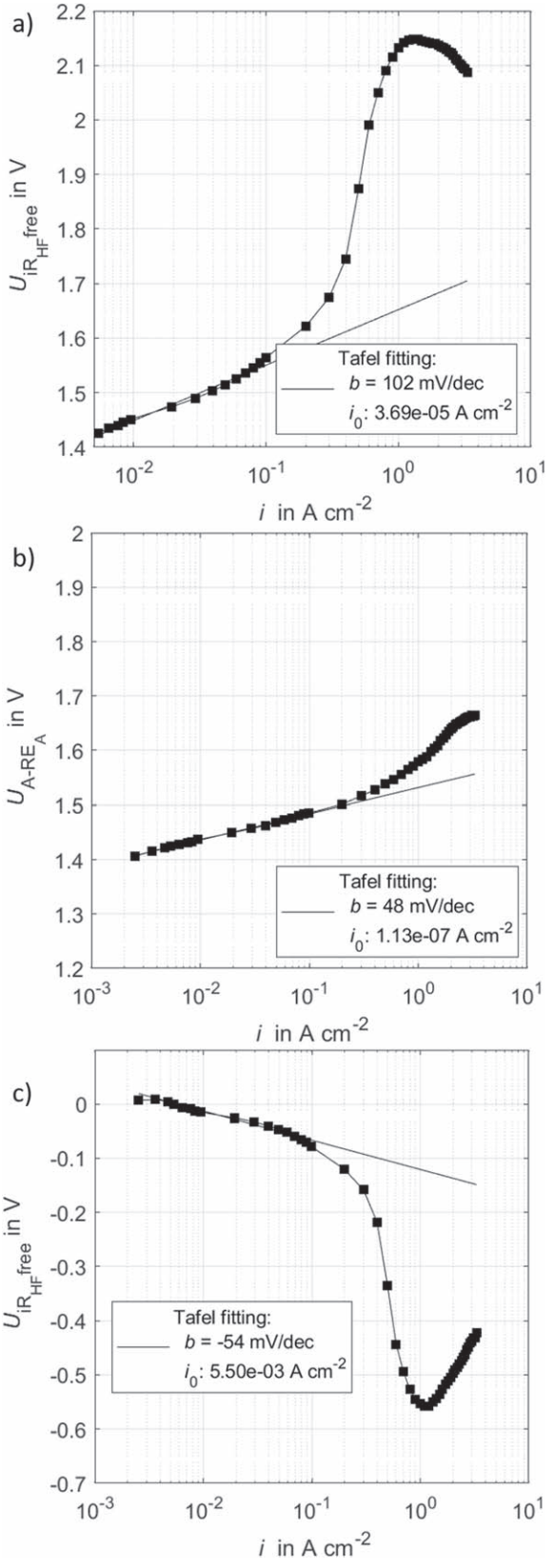

Figure 15. Measurement results for a low-performance cathode CL. (a) HFR corrected polarization curve over logarithmic current density and full cell Tafel analysis, (b) A-RE_A voltage signal over logarithmic current density and OER Tafel analysis, (c) HFR corrected RE-C voltage signal over logarithmic current density and HER Tafel analysis.

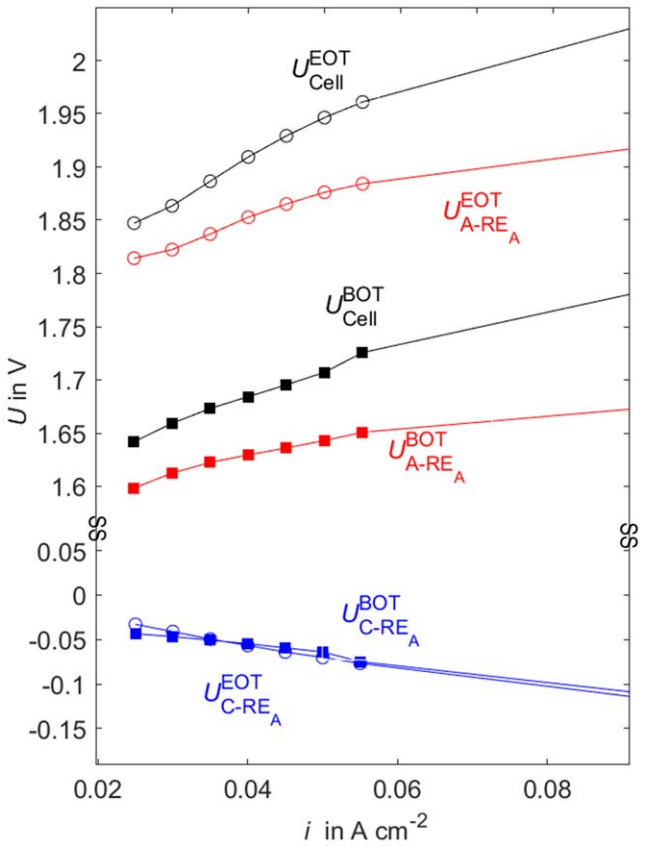

Figure 16. Cell and half-cell voltages for a degrading anode with RE at anode. Filled marks represent BOT, blank marks represent EOT.

SBRE is a crucial tool to enable catalyst investigation e.g., degradation studies.

Acknowledgments

The authors gratefully acknowledge the financial support by the Federal Ministry of Economic Affairs and Climate Action of Germany in the framework of HoKaWe (03EI3029B) and the Federal Ministry of Education and Research in the framework of Rainbow (01DG20009), Dorian Hüne, Research Center Energy Storage Technologies TU Clausthal, for expertise in SEM and EDX, Jan Gerrit Eckert, Institute of Physical Chemistry and Electrochemistry LUH, for support in PTL material preparation, Agate Martin, Institute of Electric Power Systems LUH, for expertise in electrochemical measurement setups and the fruitful discussions, Torben Gottschalk, Institute of Electric Power Systems LUH, for support in hydrogen pump experiment, Chuyen Van Pham, Simon Thiele, and Anna Freiberg, Forschungszentrum Jülich GmbH, Helmholtz Institute Erlangen-Nürnberg for Renewable Energy (IEK-11), for providing CCMs for experiments regarding additional use cases. The project has in parts, been funded by the Deutsche Forschungsgemeinschaft (DFG, German Research Foundation) under Germany's Excellence Strategy within the Cluster of Excellence PhoenixD (EXC 2122, project ID: 390833453).

ORCID

Lena V. Bühre https://orcid.org/0000-0002-8555-703X
Boris Bensmann https://orcid.org/0000-0001-8685-7192

References

1. K. E. Ayers, N. Danilovic, K. W. Harrison, and H. Xu, *Electrochem. Soc. Interface*, **30**, 67 (2021).
2. K. Ayers, *Current Opinion in Electrochem.*, **18**, 9 (2019).
3. D. Bessarabov, H. Wang, H. Li, and N. Zhao (ed.), *PEM Electrolysis for Hydrogen Production* (Boca Raton, FL, CRC Press) (2015).
4. T. Schuler, T. J. Schmidt, and F. N. Büchi, *J. Electrochem. Soc.*, **166**, F555 (2019).
5. T. Smolinka, E. Ojong, and T. Lickert, *PEM Electrolysis for Hydrogen Production*, ed. D. Bessarabov, H. Wang, H. Li, and N. Zhao (Boca Raton, FL, CRC Press) 11 (2015).
6. A. Hartig-Weiß, M. Bernt, A. Siebel, and H. A. Gasteiger, *J. Electrochem. Soc.*, **168**, 114511 (2021).
7. E. Brightman, J. Dodwell, N. van Dijk, and G. Hinds, *Electrochem. Commun.*, **52**, 1 (2015).
8. O. Sorsa, J. Nieminen, P. Kauranen, and T. Kallio, *J. Electrochem. Soc.*, **166**, F1326 (2019).
9. A. A. Kulikovsky and P. Berg, *J. Electrochem. Soc.*, **162**, F843 (2015).
10. D. Gerteisen, *J. Appl. Electrochem.*, **37**, 1447 (2007).
11. H. Kuhn, B. Andreaus, A. Wokaun, and G. G. Scherer, *Electrochim. Acta*, **51**, 1622 (2006).
12. G. Hinds and E. Brightman, *Electrochem. Commun.*, **17**, 26 (2012).
13. H. Becker, L. Castanheira, and G. Hinds, *J. Power Sources*, **448**, 227563 (2020).
14. G. Tsotridis and A. Pilenga, *Eu Harmonized Protocols For Testing Of Low Temperature Water Electrolysis* (Luxembourg, Publications Office of the European Union) (2021), https://data.europa.eu/doi/10.2760/58880.
15. A. Martin, P. Trinke, M. Stähler, A. Stähler, F. Scheepers, B. Bensmann, M. Carmo, W. Lehnert, and R. Hanke-Rauschenbach, *J. Electrochem. Soc.*, **169**, 14502 (2022).
16. "Fraunhofer Institute for Solar Energy Systems ISE." *Fraunhofer ISE—Annual Report 2020/2021* (2021), (Freiburg, Germany).
17. A. W. Bott, "Practical Problems in Voltammetry 3: ReferenceElectrodes for Voltammetry." *Current Separations*, **14**, 2 (1995).
18. A. Martin, P. Trinke, C. van Pham, M. Bühler, M. Bierling, P. K. R. Holzapfel, B. Bensmann, S. Thiele, and R. Hanke-Rauschenbach, *J. Electrochem. Soc.*, **168**, 114513 (2021).
19. M. Suermann, T. J. Schmidt, and F. N. Büchi, *Electrochim. Acta*, **211**, 989 (2016).
20. C. M. Zalitis, J. Sharman, E. Wright, and A. R. Kucernak, *Electrochim. Acta*, **176**, 763 (2015).
21. M. Suermann, B. Bensmann, and R. Hanke-Rauschenbach, *J. Electrochem. Soc.*, **166**, F645 (2019).
22. P. Mazúr, J. Polonský, M. Paidar, and K. Bouzek, *Int. J. Hydrogen Energy*, **37**, 12081 (2012).
23. M. Carmo, D. L. Fritz, J. Mergel, and D. Stolten, *Int. J. Hydrogen Energy*, **38**, 4901 (2013).
24. H. Ohno, S. Nohara, K. Kakinuma, M. Uchida, A. Miyake, S. Deki, and H. Uchida, *J. Electrochem. Soc.*, **164**, F944 (2017).
25. T. Lazaridis, B. M. Stühmeier, H. A. Gasteiger, and H. A. El-Sayed, *Nat. Catal.*, **5**, 363 (2022).